Engineering Structures 241 (2021) 112410

Contents lists available at ScienceDirect

Engineering Structures

journal homepage: www.elsevier.com/locate/engstruct

Hysteretic behavior of repaired C-shaped concrete filled-composite plate shear walls (C-PSW/CF)

Emre Kizilarslan *, Michel Bruneau

Dept. of Civil Structural and Environmental Engineering, Univ. at Buffalo, Buffalo, NY 14260, United States

ARTICLE INFO

Keywords:
Repair
Composite plate shear walls
Cyclic testing
Inelastic behavior
Flexural behavior
Ductility
Plate buckling
Fracture
Strength degradation

ABSTRACT

Composite Plate Shear Wall/Concrete Filled (C-PSW/CF) have been the subject of much recent research for application as core-walls in high-rise construction. This lateral-force resisting system consists of steel plates connected with tie bars and "sandwiching" concrete between them. Previous tests on C-shaped C-PSW/CF walls Kenarangi et al. (2020) that were subjected to flexure and axial loads together showed a good cyclic behavior without premature strength degradation. For the specimens tested, axial load as high as 19% of the crushing load of the infill concrete ($A_c f'_c$) was applied. Also, ductility was observed to be more than 4 when flexural strength dropped to 80% of its peak values. Another perceived advantage of these type of walls was that repair was believed to be easier to repair following earthquake damage, but no repair strategy had been formulated and verified in the past. The availability of a damaged specimen as a results of the Kenarangi et al. (2020) tests provided an opportunity to develop a proposed structural repair scheme and investigate it effectiveness. Such a repair scheme was implemented on one of the damaged specimens that was then retested. The repair process and results from testing of that repaired specimen are presented in this paper.

1. Introduction

Composite Plate Shear Wall/Concrete Filled (C-PSW/CF) have recently gained much attention for application as core-walls in high-rise construction. This lateral-force resisting system consists of steel plates "sandwiching" concrete. The steel plates are typically connected to each other using tie bars (Fig. 1).

Similarly to reinforced concrete shear walls in high rise buildings, C-PSW/CF can be used with coupling beams – albeit, composite coupling beams in this case. Among the benefits of this structural systems, steel panels of C-PSW/CF can be fabricated off-site and can serve as formwork for the concrete, which has been reported to speed up construction time [1]. This structural system has been used in mid-rise construction in non-seismic regions [2], as well as in nuclear structures [3–5], but application to buildings in seismic regions is new. The cyclic inelastic non-linear behavior of this structural system was investigated by testing two large scale C-shaped [6] and five planar C-PSW/CF walls [7] at the University at Buffalo and Purdue University, respectively. These walls were subjected to both flexure and axial loads, and the experiments allowed to establish their strength, cyclic ductility, and drift capacity.

The tests (Fig. 2) done at the University at Buffalo showed that C-shaped C-PSW/CF walls exhibited good cyclic behavior without premature strength degradation; these specimens were subjected to large axial load of up to 19% of the crushing load of the infill concrete ($A_c f'_c$). Also, ductility was more than 4, and specimens reached or exceeded their calculated plastic moment capacities in the positive and negative directions. At the end of the tests, the flexural strength was observed to be 4138/–2503 *kip-ft.* (5610/–3394 *kN*-m). Buckling occurred between multiple layers of tie bars, as a result of yielding over a considerable part of the height. Ultimately, fracture of the steel plates occurred at the wall base, but flexural strength degradation was relatively slow.

Another perceived advantage of these types of walls is that repair was believed to be easy after earthquake, even if in cases of damage, no repair concept had been formulated or experimentally verified. The availability of a damaged specimen from the Kenarangi et al. [6] tests provided an opportunity to experimentally investigate a possible structural repair scheme and its effectiveness. Therefore, a repair scheme was developed and implemented on that damaged specimen, which was then subjected to a repeat of the testing protocol, for comparison of the resulting behavior with that of the original virgin specimen. This was done with the second C-shaped specimen of the previous testing program [6]. That specimen had been subjected to cyclic lateral

* Corresponding author.
E-mail addresses: emrekizi@buffalo.edu (E. Kizilarslan), bruneau@buffalo.edu (M. Bruneau).

https://doi.org/10.1016/j.engstruct.2021.112410
Received 2 December 2020; Received in revised form 22 March 2021; Accepted 14 April 2021

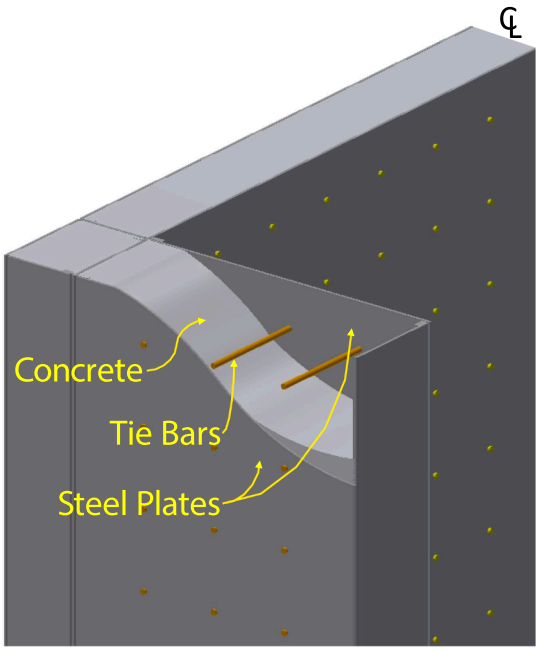

Fig. 1. Component of Composite Plate Shear Wall/Concrete Filled.

load simultaneously with a constant axial load equal to 15% of the crushing load of the infill concrete (i.e., $0.15A_c f'_c$ (referred to as Specimen C2). That specimen had also been tested, on purpose, up to extreme inelastic deformations to investigate the rate of strength degradation at progressively larger drifts; by all means, significantly lesser damage would be expected following actual earthquakes. However, the objective in the repair scheme considered here was to restore the flexural strength and to achieve ductile response comparable to that of the original specimen. Performing this repair on an extremely damaged specimen would provide confidence that this could be evidently achieved for lesser damaged specimens. This paper presents the proposed concept used to repair the Specimen C2 wall and results from its retesting after repair. This paper presents the details of the repair procedure used and implemented here, as well as results and findings on the cyclic, nonlinear, inelastic response of these repaired walls.

2. Previously tested specimen to be repaired

Fig. 2a shows the 3D view of the test setup and Specimens C1 and C2 tested by Kenarangi et al. [6], together with the cross-section of the walls (Fig. 2b). The test setup consisted two servo-hydraulic actuators to apply axial loading to the wall, and two horizontal actuators to apply lateral loading, as shown in that figure. The base of the walls was embedded 2 *ft.* (610 *mm*) inside of a footing to transfer the base moment and shear to the laboratory strong floor. As part of the footing reinforcement, some #10 bars ran through holes (Fig. 2c) in walls' flanges (Fig. 2b) to help anchor the walls into the footing, and 3/8 *in.* (9.53 *mm*) thick plates (labelled "Thicker Plate" in Fig. 2c were used for the part of the wall embedded in the footing to prevent yielding of the wall there (particularly between the holes where the #10 reinforcing bars ran). At the bottom of the wall, a base plate and stiffeners detail was used as the primary mechanism to anchor the wall in the foundation; note that this is a detail similar to the one used by other researchers [8–10]. Moreover, 1–3/8 *in.* in diameter DYWIDAG bars were post-tensioned to the laboratory's strong floor to keep the walls in place.

The walls were made of 3/16 *in.* (4.76 *mm*) steel plates connected with 0.5 *in.* (127 *mm*) diameter tie bars spaced at 6 *in.* (152 *mm*) in both the horizontal and vertical directions. They had the following dimensions and properties: wall height, $H = 174$ *in.* (4420 *mm*); flange length, $h = 97.5$ *in.* (2476.5 *mm*); web length, $b = 30$ *in.* (762 *mm*); steel plate thickness, $t = 0.1875$ *in.* (4.76 *mm*); flange thickness, $d = 6$ *in.* (152.4 *mm*); web thickness, $c = 8.375$ *in.* (212.73 *mm*); tie spacing = 6 *in.* (152.4 *mm*); tie diameter = 0.5 *in.* (12.7 *mm*); wall aspect ratio, $H/b = 5.53$; cross-section aspect ratio, $\gamma = b/h = 0.31$; flange aspect ratio, $\alpha = d/h = 0.06$; web aspect ratio, $\beta = c/b = 0.28$; steel area, $A_s = 61.8\text{in}^2$ (39871 mm^2); concrete area, $A_c = 9225.2\text{in}^2$ (5951730 mm^2); reinforcement ratio of web, $\rho_{web} = 4.5\%$; reinforcement ratio of flange, $\rho_{flange} = 6.3\%$, and; reinforcement ratio, $\rho_s = 6.3\%$. The length of the tie bars in the flanges was 6.375 *in.* (162 *mm*), and in the webs 8.75 *in.* (222.25 *mm*) (and 0.375 *in.* (9.53 *mm*) longer inside the footing to accommodate the thicker plate used there). Moreover, the Thicker Plates were connected to wall's steel plates with complete joint penetration (CJP) welds.

To transfer axial loading to the specimen, an axial loading top fixture (consisting of an inverted T-shape plate with stiffeners) was designed and placed on top of flange of the wall to apply forces from the vertically inclined actuators to the walls. The actuators were placed at a 70° angle from the laboratory's strong floor. For the lateral loading setup, two actuators were used. More details can be found in Kenarangi et al. [6].

3. Selected repair strategy

Seeking a repair strategy that is practical and applicable for post-earthquake repairs, irrespective of the severity of wall damage, it was determined from a practical perspective that composite walls would likely be repaired in segments, and that the repair would involve replacement of the buckled plates and, if necessary, partial or complete replacement of the concrete located between the removed plates. In the case of repair to extreme damage, complete concrete replacement and new ties would be used, whereas existing ties would be re-used in the case of partial concrete replacement. The outcome of repair concept would be new plates offset from the original position, as schematically illustrated in Fig. 3, but stronger than the original ones, with the intent of moving the plastic hinge location above the repair location in future extreme earthquakes. After the repair concept proposed and investigated here was developed by the research team, discussions were held with the contractors (Turner Construction Company) and steel erector (James F Stearns Co Inc.) partnering on this project to establish a workable construction process and details needed to achieve the repair objectives.

The repair was accomplished on Specimen C2 tested by Kenarangi et al. [6]. In that Specimen C2, after the wall had been cycled to +6.25/−5.36% drift (+0.052/−0.044 rad rotation), webs of the wall (Fig. 2b) were buckled up to the 4th tie bar row and extensively fractured between the 1st and 2nd tie bar rows. The flange steel plate on the wall's East side had buckled between the 1st and 2nd tie bar rows but there was no buckling/fracture in the flange on its West side (North direction is provided in Fig. 2a).

The repair strategy retained to address such extensive damage conceptually consisted of the following steps:

1) Chipping away a part of the concrete footing (Fig. 2a) at the face of the wall, removing enough concrete to expose the CJP weld of the wall plate to the thicker wall plate inside of footing (Fig. 3).
2) Cutting and removal of the buckled and fractured steel and removal of the loose concrete exposed by removal of the plates. This was expected to involve some chipping of the exposed concrete all around the wall, and removal of concrete through the entire thickness of the wall in some locations (such as in most of the webs).
3) Adding steel plates along the entire perimeter of wall at its base where buckled/fractured plates were removed. These new steel plates, effectively acting as splice plates, were to be fillet-welded at their top and bottom ends. At the bottom end, this would be to the existing thicker plate located inside the wall's footing, and at the top end to the existing non-damaged steel plate. Note that, at the bottom, the splice plate was fillet-welded to the thicker wall plate to "by-

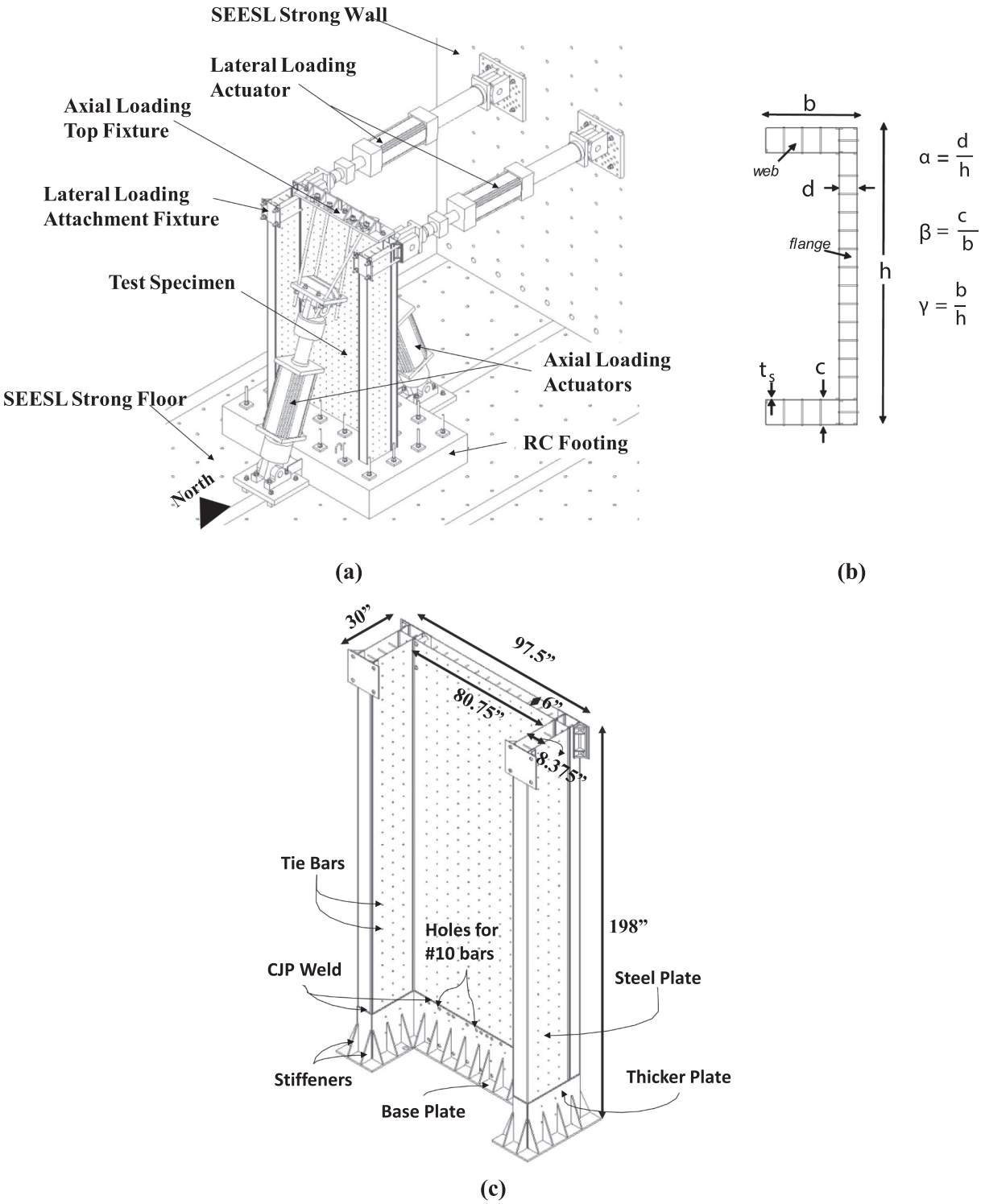

Fig. 2. (a) Test setup of C-Shaped Composite Plate Shear Wall/Concrete Filled (C-SPW/CF), (b) cross-section of the walls, and; (c) isolated wall (Note: 1 in. = 25.4 mm).

pass” the thinner plate at the wall base, in order to achieve load transfer directly to the thicker plate and ensure no yielding of the thinner plate there. The new splice would be made of plates of identical dimensions “wrapping” all around the wall, as shown in Fig. 3.

4) The empty space between the splice plates should then be filled with self-consolidating concrete that could easily flow through voids without the need for vibrations.

The thickness of the repair steel plate (splice plate) was chosen based on a number of considerations, including finite element analysis done in LS-DYNA and required fillet weld size as described below. Note that, as mentioned above, the main objective was to make the repaired section stronger, such as to develop plastic hinging above the repaired part; therefore, an added design objective was to keep the splice plates elastic.

First, the thickness of the fillet weld to the splice plate was calculated such as to be able to transfer a force equal to yielding of the steel plate in

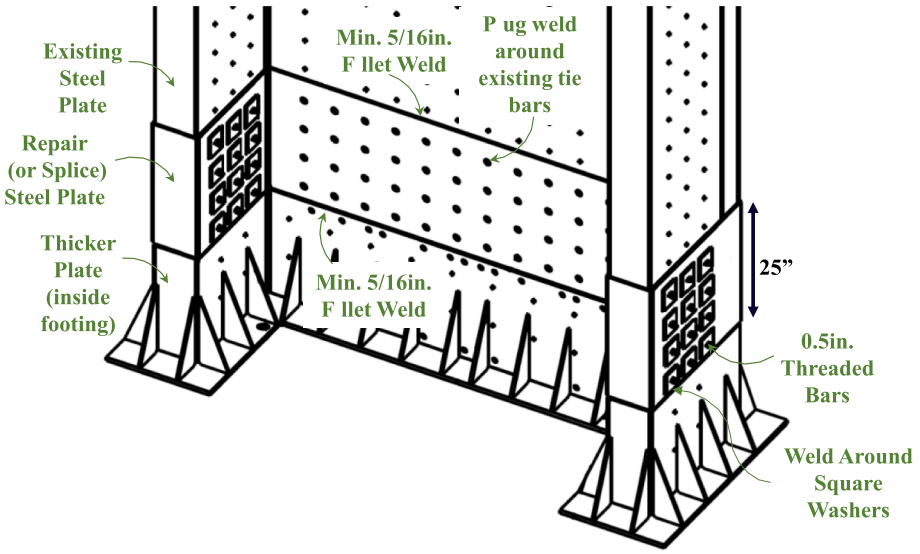

Fig. 3. Repair concept for the Specimen C2 (Note: 1 in. = 25.4 mm).

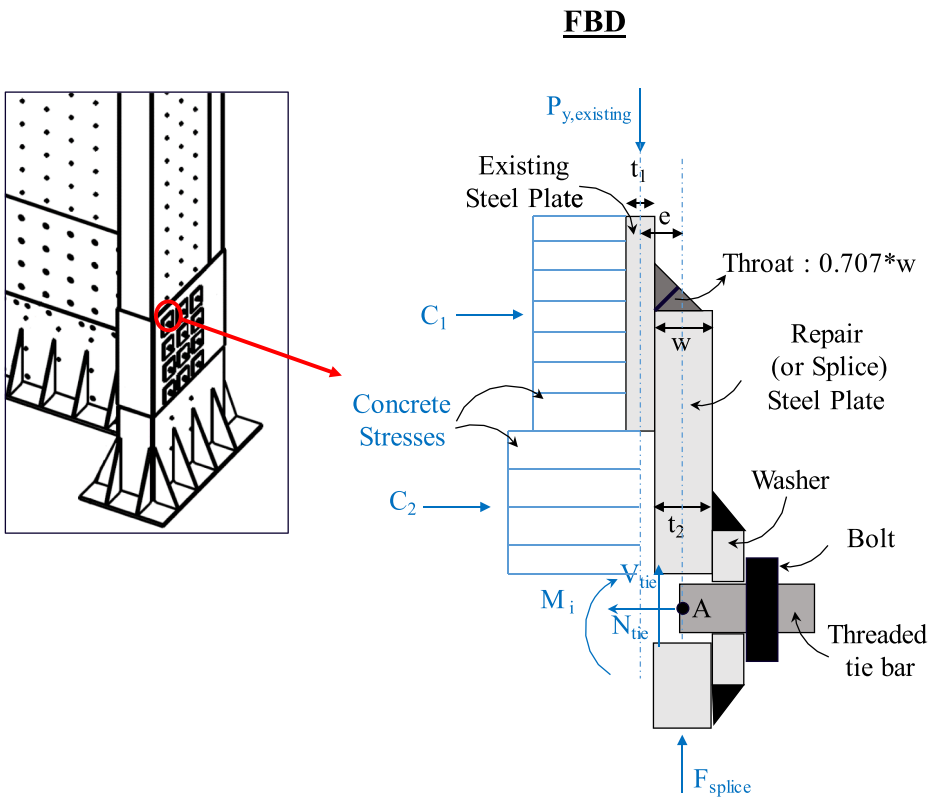

Fig. 4. Free body diagram of existing and splice plates load transfer.

the above plastic hinge region. Considering a 0.707*w throat for the fillet welds, where w is the size of the weld, the required fillet weld size was required to be at least 5/16 *in.* (7.94 *mm*), plus a 1/16 *in.* (1.59 *mm*) clear distance from the plate edge, to resist the yield force from existing steel plate. Therefore, the required thickness of the splice plate was 3/8 *in.* (9.53 *mm*), i.e., the twice the thickness of the existing plate.

Note that in an initial approach, the size of the plate was checked for its adequacy to resist the combination of compressive yield force from the plate above the splice, and the moment created by the eccentricity of that force from the middle of existing plate to the middle of the splice plate. However, under such an assumption, to keep the splice plate elastic would have required it to be 1 *in.* (25.40 *mm*) thick, which quickly appeared to be excessive. More appropriately, the splice plate thickness was selected considering the free-body diagraph shown in Fig. 4, where the moment due to eccentricity of the force is resisted by the couple developed by the concrete force resulting from stresses developing behind the plates and the force the at tie bars. Note that finite element analysis also indicated that the tie bar also resisted a moment equal to 9.5% of the plastic moment of tie bar, which is negligible. Also, note that the contribution of friction forces was neglected in this free-body-diagram, as it is not significant. Analysis using LS-DYNA confirmed that the 3/8 *in.* (9.53 *mm*) splice plate provided was adequate.

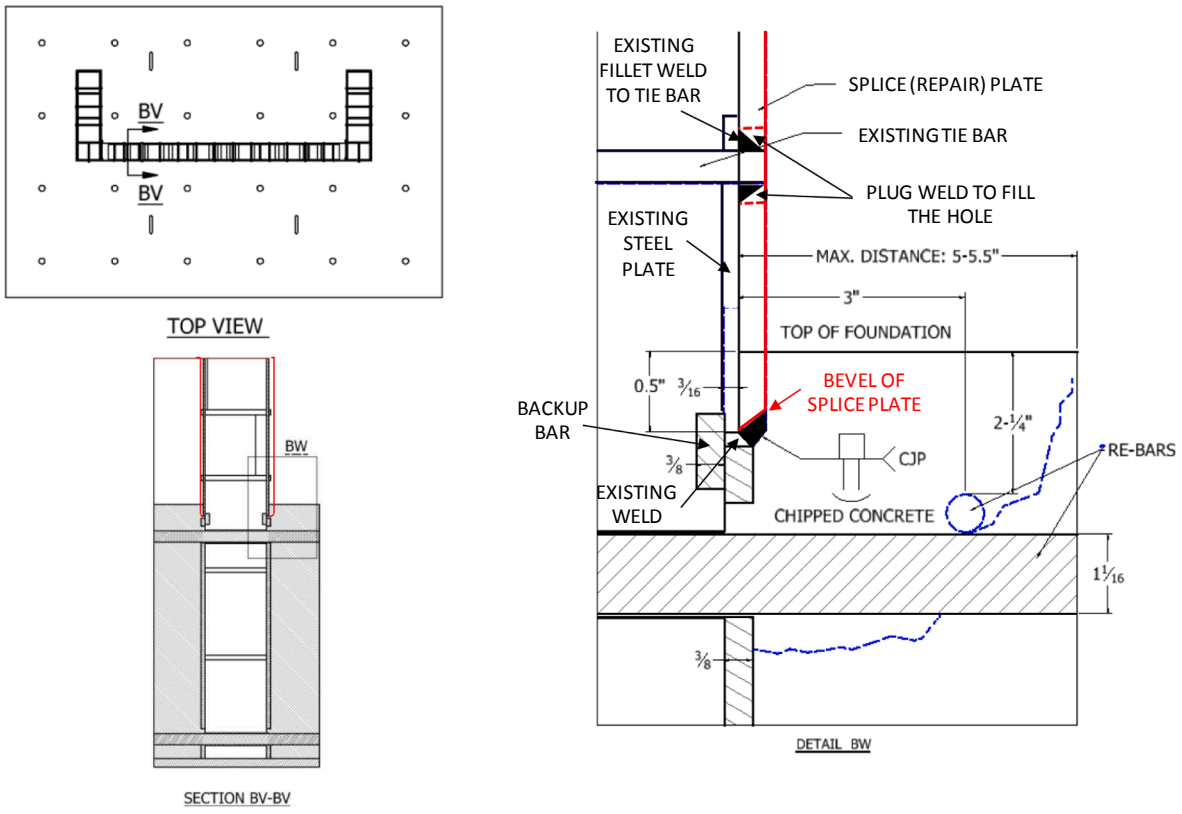

Fig. 5. Fillet welding detail at the footing.

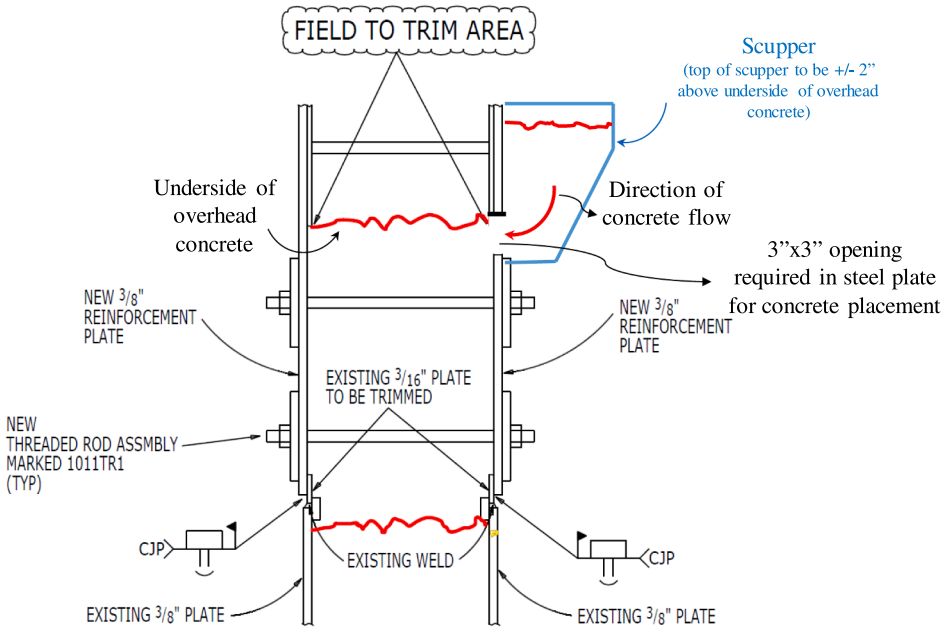

Fig. 6. Scupper attachment and direction of concrete flow.

Finally, the height of the repair plate was chosen based on the fact that the webs were damaged up to 4th tie-bar row. Even though the steel in the flange was not damaged beyond the 2nd tie-bar row, the intent was to use a splice plate of same height to provide continuity between the webs and flange and facilitate formation of a plastic hinge at the same height all around the wall. Hence, the total splice plate height was chosen to be 25 *in.* (635 *mm*) (extending 24.5 *in.* (622.3 *mm*) above the top of footing and 0.5 *in.* (12.7 *mm*) into the footing where it was connected to the thicker wall plate). Moreover, to bridge over locations of the flange where the steel plates and ties would not be removed, the splice plates were provided with a grid of pre-cut 1–3/4 *in.* (44.45 *mm*) in diameter holes located to match the exiting tie-bar spacing (6 *in.* (152.4 *mm*) c/c in both the horizontal and vertical directions).

For the implementation, there was no damage in the west flange. Therefore, a 3/8 *in.* (9.53 *mm*) repair plate having holes at the same spacing as for the existing tie bars, was placed on top of the 3/16 *in.*

Fig. 7. Repairing sequence of flanges.

Fig. 8. Repairing sequence of webs.

(4.76 *mm*) existing steel plate. The top and bottom of the repair plate were fillet-welded to the existing plate and the tie bars were plug-welded to the repair plate around the holes. On the east flange, where the steel in 1st and 2nd tie-bar row had buckled during the prior test, the same approach was used, except that the buckled steel was cut out prior to application of the repair plate. This cutout was done in a way that left some steel around the tie bars were left for plug welding. Also, the damaged concrete behind the buckled steel was removed (approximately 3 *in.* (76.2 *mm*) of the wall thickness) prior to adding the splice plate. Note that in order to facilitate welding the splice plate to the thicker plate inside the footing, the bottom of the splice plates was beveled, as shown in Fig. 5. After that, three 3 *in.* × 3 *in.* (76.2 *mm* x76.2 *mm*) holes were cut in the middle of 1st and 2nd tie-bar rows, 3 *ft.* (914.4 *mm*) apart from each other. Scuppers were attached to the surface of the plate with screws; these were wood boxes with an opening at their bottom attached to the surface of the wall, where the 3 *in.* × 3 *in.* (76.2 *mm* x76.2 *mm*) holes were located (as shown in Fig. 6). Then, a MasterEmaco S-440CI self-consolidating repair mortar with 3/*8in.* (114.3 *mm*) aggregate, integral corrosion inhibitor and high workability was poured through scuppers. During pouring, the plate was tapped with hammers to generate vibration to help fill all voids. Filling the scupper to the top created enough pressure to fill all empty space of chipped concrete. To further confirm that the concrete reached the top of the cavity, this was also checked by hand (with fingers through the holes as far as could reach), and by concrete leakage from small holes of 1/8 *in.* (38.1 *mm*) diameter, that were drilled at the top level of chipped concrete on the far ends and middle of the splice plates. Then, the lids of the scuppers were slid to close the holes. Next day, the scuppers were removed and the surface was cleaned. Finally, the opened spots were capped by welding around slightly bigger plates (Fig. 7).

The damage on both north and south webs spread up to four rows of tie-bars (Fig. 8). Therefore, the same repair strategy was applied to both webs, which consisted of removing the steel plates, concrete and tie-bars in the damaged area, and installing new ones. The steel plate was flame-cut first. Then, the concrete and tie-bars were removed with concrete chipping machines (i.e., jack hammers). The repair plates were positioned in-place and fillet welded at their top and bottom. Then, 0.5 *in.* (152.4 *mm*) diameter threaded rods were placed through pre-cut holes in the repair plates and washers were put on each side of the webs and tightened with bolts. In order to prevent concrete leakage, the washers were welded around the plate. Then, concrete was poured through a scupper that was mounted to a pre-cut hole (3 *in.* × 3 *in.* (76.2 *mm* × 76.2 *mm*)) on the cap plate, as described above for the flange. The same procedure was followed, except that, in this case the 1/8 *in.* (38.1 *mm*) holes were drilled at the end of web, close to the corners of the wall.

Concrete cylinders cast with the material used for the repair were periodically tested until the strength reached was at least equal to the value of the concrete on the day of the initial test on Specimen C2. Meanwhile, all remaining aspect of test set-up and instrumentation were completed (Fig. 9).

Fig. 9. Test setup of Repaired Specimen C2.

4. Material properties of repaired specimen C2

Steel coupons for the webs and flange of the C2 specimen, as well as for the repair plates, were tested under uniaxial tension. A572Gr50 steel was specified for the flange and web plates of Specimen C2, but no "yield plateau" was obtained in the resulting stress–strain behavior of the coupons. The yield strengths of the web and flange plates were calculated to be 52.65 *ksi* (363 *MPa*) and 57.79 *ksi* (398.44 *MPa*), respectively, using the 0.2% offset method, resulting in an average yield strength of the plate for Specimen C2 of 55.2 *ksi* (380.59 *MPa*). Moreover, three coupons were tested in order to measure the properties of the repair steel plate. The 3/*8 in.* (2.59 *mm*) thickness of these plates was too large for the MTS uniaxial tension/compression machine inside the SEESL Laboratory at the University at Buffalo. Therefore, the thickness of the plates was machined down to half the original thickness. Unfortunately, during the test, two of the coupons broke outside of their gauge length. However, the average of the yield strength obtained for these three coupons, measured as 53.14 *ksi* (366.39 *MPa*), is sufficient to show that the repair plates has adequate strength to prevent yielding in the splice itself.

To establish strength of the concrete used for the repairs, 3 *in.* 6 *in.* (76.2 *mm* × 152.4 *mm*) and 6 *in.* 12 *in.* (152.4 *mm* × 304.8 *mm*) cylinders were taken from concrete used to fill the space between the steel splice plates on the day of concrete pouring. Average compressive strength was measured to be 6.4 *ksi* (44.13 *MPa*) from unconfined compression test. Moreover, the strength of the existing concrete inside of the Specimen C2 was determined using three extra 6 *in.* × 12 *in.* (152.4 *mm* × 304.8 *mm*) cylinders that had been cast the same day as the C2 wall; test of these cylinders indicated that the strength of concrete had not increased since the day C2 was tested, as the average strength obtained was still 5.1 *ksi* (35.16 *MPa*).

5. Loading protocol

The axial loading applied to the repaired specimen was the same as for the previously tested Specimen C2, which was 15.9% of the crushing load of the infill concrete ($A_c f'_c$). For cyclic loading, the loading protocol was based on two displacements; first and equivalent yield displacements. The first yield displacements were $\Delta_y = 1$ *in.* (25.4 *mm*) and −0.5 *in.* (−12.7 *mm*), respectively, in the positive (webs in compression) and negative (flange is in compression) loading directions, as defined by an LS-DYNA pushover analysis of a model of the specimen and test setup [6]. The equivalent yield displacements (Δ_y') were calculated as 2.0 *in.* (50.8 *mm*) and −1.5 *in.* (38.1 *mm*) in positive and negative directions based on the bilinearization of the pushover curve obtained from the same FEA model of the test setup with the measured material properties of steel and concrete for both the existing and repaired parts of the wall, respectively. Note that for similar displacement demands at the top of the wall, slightly larger rotation were expected in the repaired wall as its plastic hinge was located higher than for the non-repaired wall. The resulting cyclic displacement protocol is shown in Fig. 10. For safety reasons, drifts were limited to 6%, as the specimen had exhibited substantial strength degradation at that point.

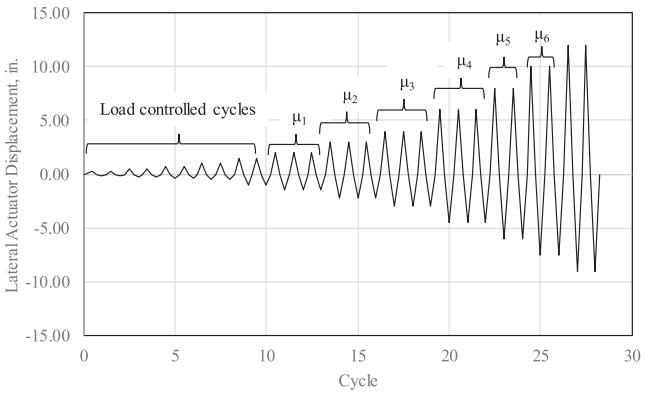

Fig. 10. Loading protocol for Repaired C-Shaped specimen.

6. Application of axial loading on the specimens

Due to practical constraints, the axial loading resultant was applied centered on the top of specimens' flange rather than at the section centroid located at $\bar{y} = 9.11$ *in.* (231.4 *mm*) from the outside face of the flange (Fig. 2b). This eccentricity of the axial load with respect to the centroid of the cross-section was duly considered when post-processing the experimental results. Also, the horizontal actuators were "locked" to restrain lateral movement of the specimens due to this eccentricity during application of the axial load.

The two vertical MTS 243.90T actuators with a nominal capacity of 450 *kips* (2002 *kN*) in tension were driven in a force-controlled mode such as to apply constant axial force to the specimen cross section. The summation of the axial force in the vertical actuators was tracked during test to verify that it remained constant throughout tests. The distribution of axial strains across the cross section were also tracked after engaging the vertical actuators, to verify that the cross-section was subjected to uniform stresses under the applied axial loading, even though loading was only applied to the flange (as previously predicted by finite analysis and also observed in the original test of the virgin specimen). Results obtained from the strain gauges located in the plastic hinge region of the specimen confirmed that this was the case.

7. Test results and observations

With the horizontal actuators "locked" at zero displacement, the test started by loading each of the vertical actuators with force of 400 *kips* (1779 *kN*). This added-up to an axial force equal to 15.9% of the concrete crushing load capacity, $A_c f'_c$, on the cross-section of the wall. Then, lateral cyclic displacements were applied at the top of the specimen following the cyclic protocol. The first cycle, at a displacement of $\Delta_y/4$,

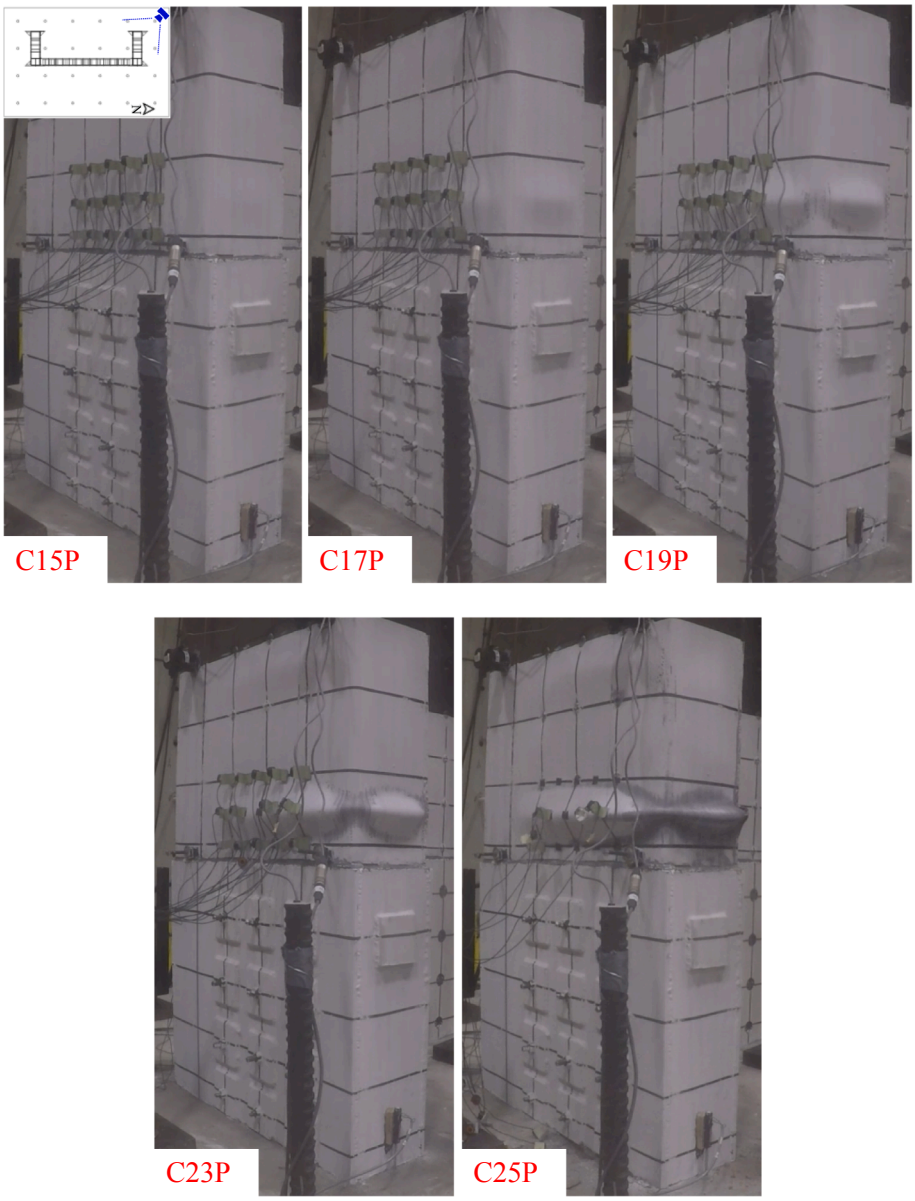

Fig. 11. Local buckling in Repaired Specimen C2 at different displacements cycles and locations: (a) the North Face of North Web (NWN), (b) the South Face of South Web (SWS), and; (c) The East face of Flange (FE).

was used to verify that all recording instruments and the test setup functioned as intended. In the early cycles, up to Δ_y, no steel plates were observed to experience buckling or yielding.

7.1. Buckling (Cycles 14 to 17)

The strain gauges confirmed linear strain profiles at specific elevations along the cross-section, up to the yield displacement of Δ_y. At the positive estimated yield displacement of Δ_y, the strains of −1305.8 and 424.5 μstrain were recorded at the farthest end of the web and flange, corresponding to 101.6 and 21.8% of the average yield strain (i.e., 1951μstrain) obtained from the coupon tests, for Specimen C2. Similar values were recorded during the second excursion at the same drift, and local buckling was still not observed.

Visual observation of buckling first occurred during the second excursion of $1.5\Delta_y'$ (3.0 *in.* (76.2 *mm*)/−2.25 *in.* (57.2 *mm*)) displacement (i.e., Cycle 14). This buckling occurred on the steel plate between the 1st and 2nd tie rows on both the South face of the North Web (NWS) and North face of South Web (SWN). Moreover, steel at 4 *in.* from the top of the repair plate also started to buckle on the West surface of North web (NWW). During the third excursion at that peak displacement (i.e., Cycle 16), buckling was also observed to initiate on the steel plate between the 1st and 2nd tie rows at the North face of the North Web (NWN) and the steel located at 4.5 *in.* and 11 *in.* from the top of the repaired part on the West surface of South web (SWW) also started to buckle (C16P in Fig. 11a). During the cycles at $2\Delta_y'$ (i.e., Cycle 17 with amplitude of 4 *in.* (101.6 *mm*) and −3 *in.* (76.2 *mm*)), the lateral strength of Repaired Specimen C2 reached the maximum values of 427 *kips*/−197 *kips* (1899.4 *kN*/−876.3 *kN*) in the positive and negative drift directions, respectively. Moreover, the steel plate between 1st and 2nd

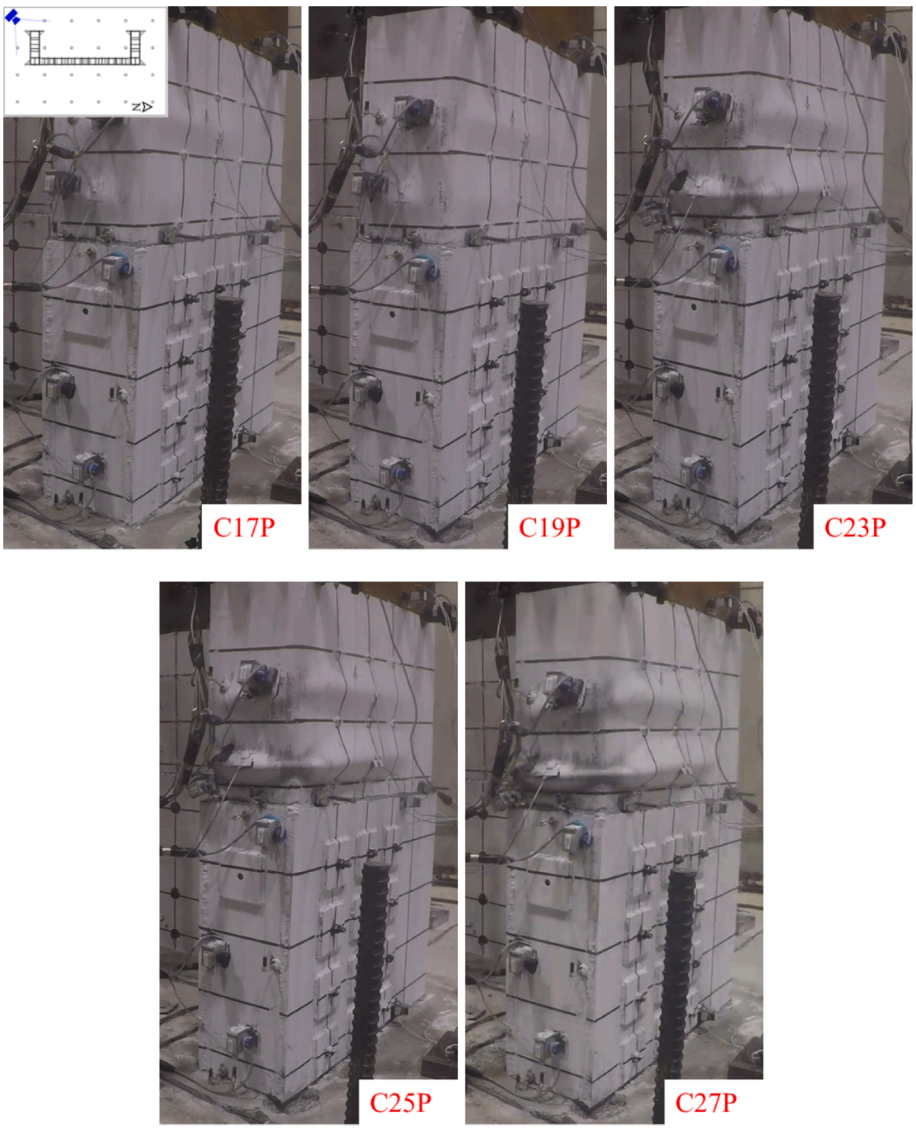

(b)

Fig. 11. (*continued*).

tie bar row on the South face of the South Web (SWS) started to buckle (C17P in Fig. 11b).

7.2. Onset of fracture and continued buckling (Cycles 18 to 19)

During the negative drift part of Cycle 17 with amplitude of 4 *in.* and −3 *in.* (101.6 *mm* and −76.2 *mm*), at 0.5 *in.* (12.7 *mm*) drift, some noticeable upward differential movement of the wall compared to the top of the footing (referred to as "uplift" hereafter) was observed at South Web (SW). Also, there was a sudden drop in the applied horizontal load. This uplift and load drop were suspected to be due to a weld fracture at the connection between the repair plate and the existing thicker plate embedded inside the footing but this could not be confirmed without chipping the concrete in the footing. Also, during next cycle, the uplift of the wall relative to footing at SW was observed to increase. At that time, a small part of the footing was chipped off, which allowed to visually confirming that the weld connecting the repair plate to the thicker plate fractured.

In the second excursion at the cyclic amplitude of +4 *in.* (102 *mm*)/ −3.0 *in.* (76 *mm*) (i.e., Cycle 18), the steel plate between 2nd and 3rd rows buckled on the East flange (labeled FE afterwards) for about 27 *in.* from the North side of the wall in the negative direction as in C18N in Fig. 11c. Buckling was also visually observed to initiate on the steel plate at the East face of the Flange (FE) between the 1st and 2nd tie rows in the second cycle (i.e., Cycle 18). During last excursion at the negative drift (i.e., Cycle 19), local buckling initiated on the steel plate between the 1st and 2nd tie bar rows on FE, except for the place on FE that had buckled between 2nd and 3rd tie-bar row in the previous cycle (refer to in Fig. 11c). Table 1 provides a comprehensive outline of the buckling that developed on the specimen throughout the test [11].

7.3. Fracture (Cycles 20 to 28)

In the Cycle 20, the fracture at the footing on SW increased to 11 *in.* (279.4 *mm*) into the web. Moreover, a slight uplift was also observed at the North Web (NW) but the exact amount of presumed fracture could not be determined at the time as no such fracture was visible. In the Cycle 23 with amplitude of 8 *in.* (203.2 *mm*) and –6 *in.* (152.4 *mm*), the weld on SW inside footing fractured up to flange. Moreover, fracture started to occur at the corners of NWS and NWW at the buckled location

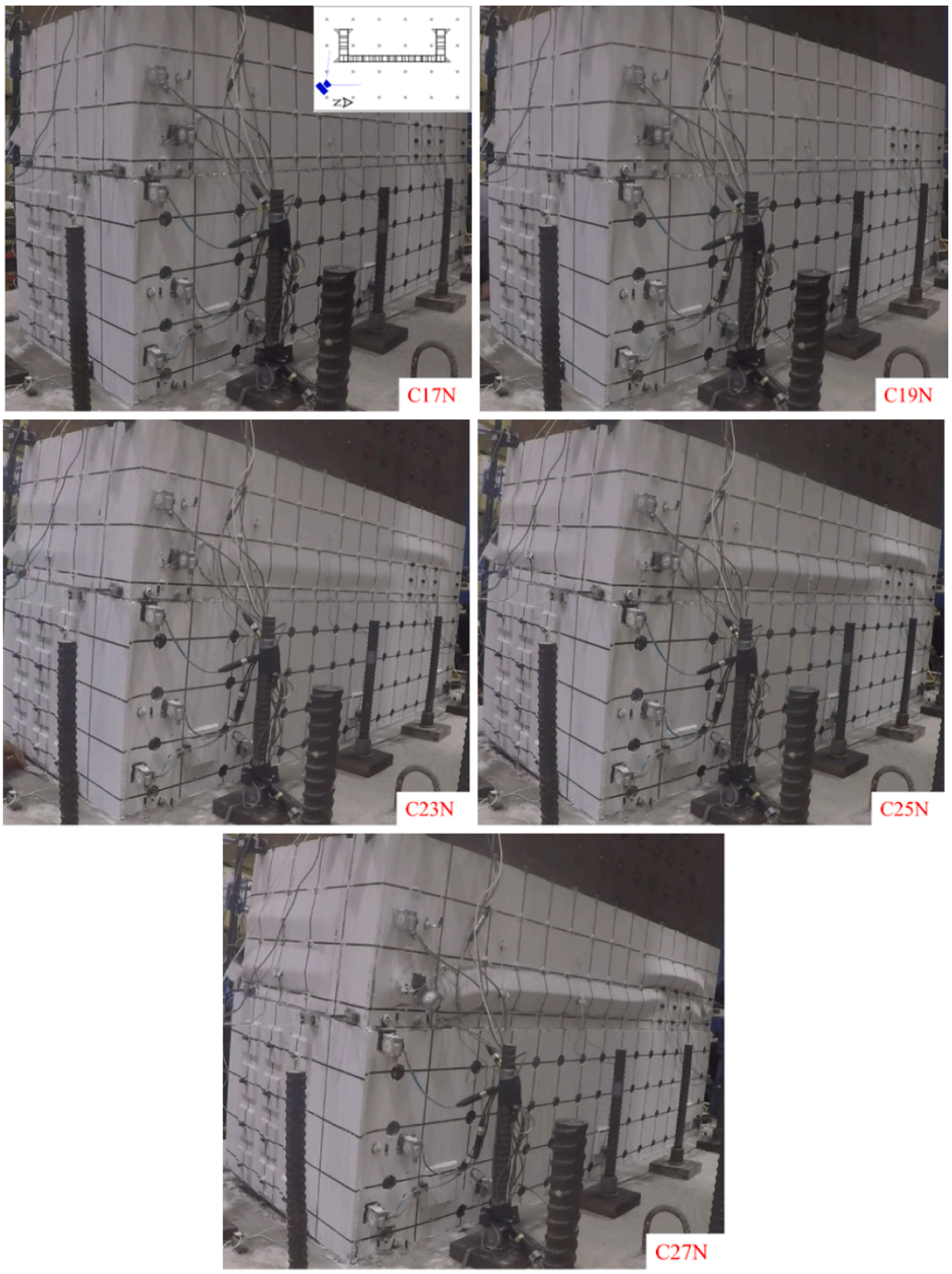

(c)

Fig. 11. (*continued*).

(4.5 *in.* (114.3 *mm*) from the top of the repair plate). The fractures were approximately 0.5 *in.* (12.7 *mm*) long at NWS; and 1 *in.* (25.4 *mm*) at NWW. After the cycle was complete, there was a 3 *in.* (76.2 *mm*) vertical fracture in the corner of NWS and NW (Fig. 13), which is a condition that has been previously encountered in rectangular end plates of composite sections (e.g., see other examples in El-Bahey and Bruneau [12], Fujimoto et al. [13], Iwata et al. [14], and Saeki et al. [15]. In the following cycle, the fracture above repair plate at NW grew and the welds around six tie bars fractured (refer to Table 1 and in [11]. In the Cycle 25 of the $5\Delta y'$ displacement (i.e., +10 *in.* (254 *mm*)/−7.5 *in.* (109.5 *mm*)), producing a reduction in lateral horizontal force applied of 20.8% and 21.06% in in the positive and negative direction, respectively. The closure plate of NW also completely and suddenly fractured. At that point, 38% of the web length (9.125 *in.* (209.6 *mm*) out of 24 *in.* (609.6 *mm*)) on the NW. Fractures progressively grew, up to the point where, at the end of test, 68.75% of the web length on NW was fractured. The test was stopped at this point. However, there were no fracture on FE and SW of the specimen above the repair plate. Other details of fracture propagation are provided in Table 1 (and in [11].

Note that Cycles 21, 22 and 28 were skipped based on the assumption that since the base of the wall was most possibly fractured; it would have not been possible to “unbuckle” the plate on the east side of the South

Table 1
Experiment log of Repaired Specimen C2 (Note: 1 in. = 25.4 mm; 1ft = 0.3048 m; 1 sq in. = 645.2 mm^2; 1 in^4 = 416231 mm^4; 1 psi = 0.0069 MPa; 1 ksi = 6.9 MPa).

Cycle No	Cycle Drift, in	Laterally Applied Force, V, kips	FE	NWW	NWN	NWS	SWW	SWN	SWS	NWE	SWE
14	3.0/-2.25	388/−173				B @1st-2nd TR		B @1st-2nd TR			
15	3.0/−2.25	381.5/−171.8		B @4in FRP	B @1st-2nd TR B @3rd-4th TR				B @2nd-3rd TR		
16	3.0/-2.25	371.6/−169.2					B @4.5in FRP B @11in FRP				
17	4.0/−3	**427/−197**					FR at footing		B @1st-2nd TR		
18	4.0	413.6									
	−3	−186.1	B @2nd-3rd TR								
19	4.0	397.1									
	−3	−182.6	B @1st-2nd TR								
20	6.0	398.7				B @2nd-3rd TR		B @3rd-4th TR			
	−4.5	−196.2		Slight upward differential movement of wall relative to top of footing (slight FR)				11in. FR at Footing		B @2nd-3rd TR	
21	6.0	n/a				**skipped**					
	−4.5	n/a									
22	6.0	n/a				**skipped**					
	−4.5	n/a									
23	8	283.8									
	−6	−165.8		1in. FR @4.5in FRP		0.5in. FR @4.5in FR	Full Web FR at Footing			B @1st-2nd TR	
24	8	230.6									
	−6	−146.1			1.5in. FR WFR @1r1c; @1r2c; @2r2c; @3r1c; @3r2c;	WFR @1r2c					
25	10.0	224.5									
	−7.5	−131.5			38% FR; WFR @2r1c on NWN						
26	10.0	193.3									
	−7.5	−111.5			52% FR						
27	12.0	212.5									
	−9	−105			68.75% FR						
28	12.0	n/a				**skipped**					
	−9	n/a									

Note: The steel plate faces are abbreviated as follows: FE = the East Flange, NWW = West of North Web, NWN = North of North Web, NWS = South of North Web, SWW = West of South Web, SWN = North of South Web, SWS = South of South Web, NWE = East of North Web, and SWE = East of South Web. Also, FF means "from footing", FRP means "from repair", FR is fracture, B is buckling, TR is tie row, WFR is tie weld fracture, r is tie row, and c is tie column. n/a means not applicable.

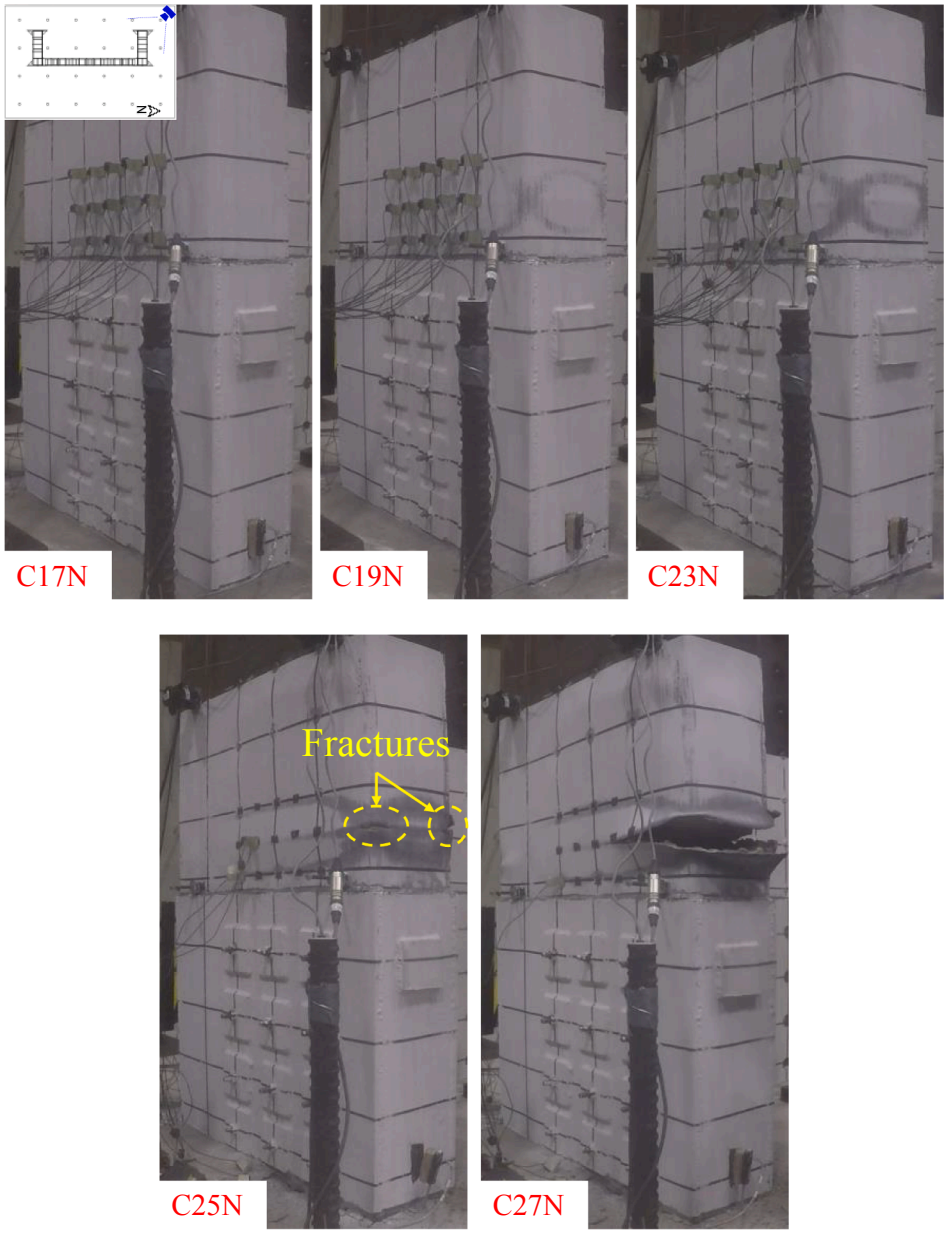

Fig. 12. Fractures in Repaired Specimen C2 at different displacements cycles and locations: (a) the North face of North Web (NWN), and; (b) the South Face of South Web (SWS).

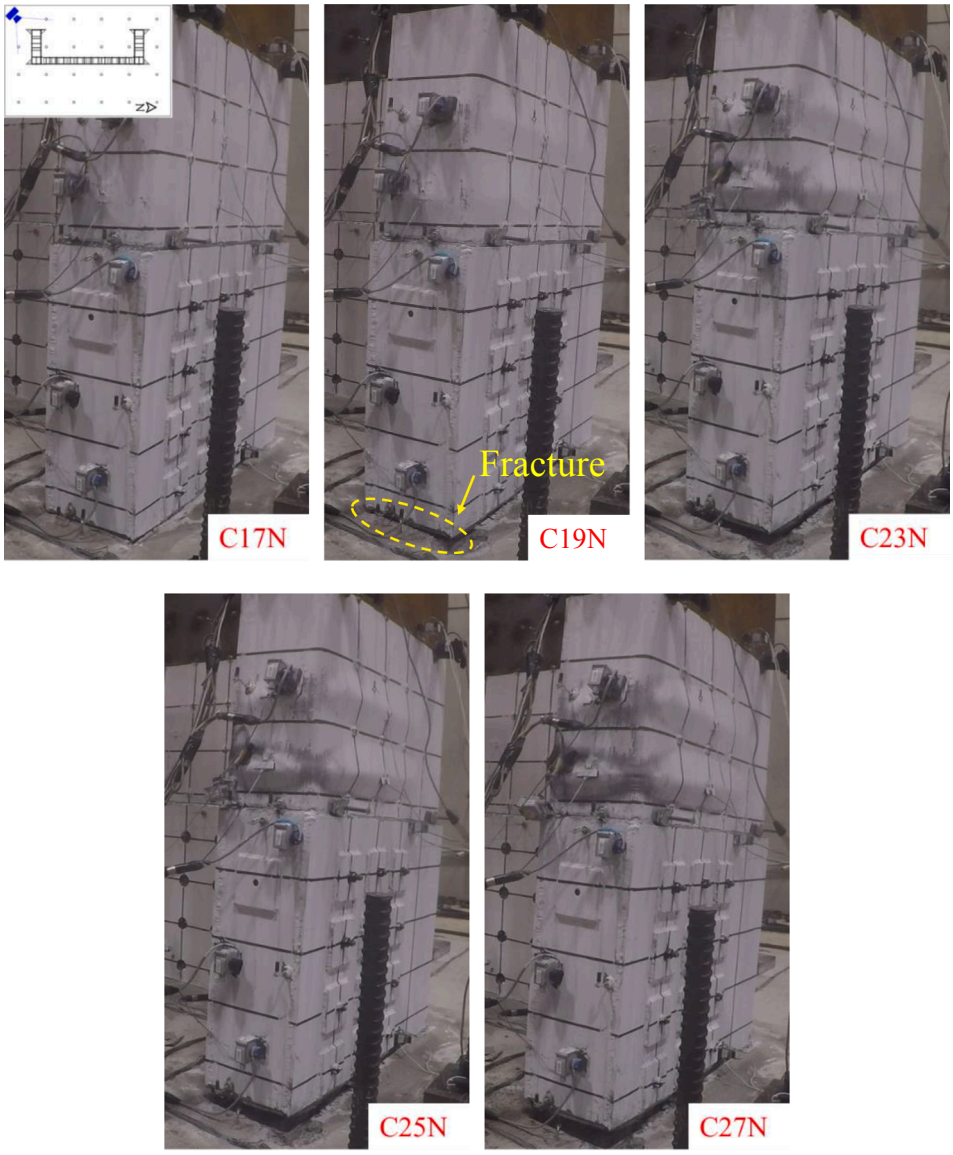

(b)

Fig. 12. (*continued*).

web with the same cyclic amplitude. However, by pushing the specimen further to a larger displacement, this would allow the specimen to buckle further and presumably help identify if failure would happen at larger displacements and see strength degradation at the same time.

The above behavior is in part captured by Fig. 11, which maps where local buckling occurred on the specimen at different peak displacements. Likewise, Fig. 12 shows fractures in Repaired Specimen C2. The labels in these figures (in the form of *CnP* and *CnN*) refer to peak positive and negative displacements during Cycle n. For example, *C15P* refers to the peak positive displacement (*P*) reached during the test's fifteenth cycle (*C15*).

Also, when the test was over, the concrete all around the webs and at the corners of the flanges in the footing was chipped off to reveal how much the fracture propagated in both webs of the wall. Fig. 14 shows the fractures of welds connecting the repair plate to the thicker plate inside of the foundation at NWS, NWN, SWN and SWS, respectively. The weld in the south web fractured almost all of the web's cross section, up to the flange (24.5 *in.* (622.3 *mm*) at SWS and 24 *in.* (609.6 *mm*) at SWN). However, the weld fractures at NWN and at NWS were shorter, at 20.5 *in.* (520.7 *mm*) and 9.25 *in.* (234.95 *mm*), respectively. The initial fractures at SWS and SWN were attributed to the fact that the location of the existing weld that connected the wall steel plate to a thicker plate in the footing, was not at the same height around the webs. Note that this thicker plate in the footing is an artifact of the experimental set-up used to prevent yielding in the footing and for needing a heavily reinforced shallow footing to be able to transfer the wall base moment to the strong floor. This heavy reinforcement created obstacles to removal of concrete in the footing. As a result, the splice plate added as part of the repair scheme ended-up to be a bit short in some places, making it difficult to weld the splice plate to thicker plate in the footing, as originally intended as part of the repair scheme (the same obstacles also challenged the welder in accessing this bottom detail). Therefore, in order to transfer loads to thicker plate inside the footing, five passes of fillet weld were done at that bottom location, trying to span the distance. However, in some places at the bottom end of the web, not enough weld material was added, and the splice plate ended-up being connected to the thinner part of the wall above the footing plate. As a results, a fracture initiated in the existing weld on the South Web. Furthermore, observation of the

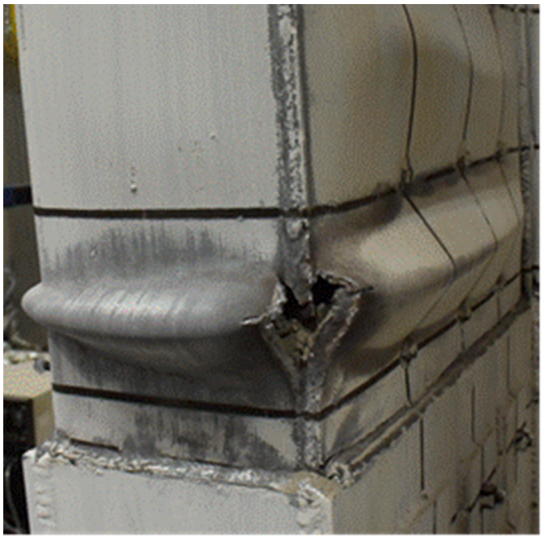

Fig. 13. Vertical weld fracture at the corner of the NWS and NWW surfaces.

fracture surface after completion of the test showed that the fracture of the new weld at that location revealed lack of fusion with the beveled splice plate, as shown in Fig. 15. In actual buildings with a number of underground levels, peak moment in the wall would be in the slab at ground level, making concrete removal in the less heavily reinforced slab around the wall easier, thus improving access to weld details and making it possible for the detail at the bottom of the reinforcing plate to be a mirror image of the detail at the top. However, the experimental results here are helpful to emphasize the need to provide a good/clean access to all critical repair locations. This facture propagated more through web during the negative drift of the Cycle 23, and did not change in the following cycles. The same phenomenon happened for the fracture at NWN, but the fracture at NWS was through the thicker plate in the footing. Note that in the laboratory setting, due to the presence of the footing, the weld connecting the splice plate to the thicker plate was difficult to accomplish, as it was hard for the welders to see the bottom of the splice plate, even though it was beveled.

8. Test results

Fig. 16 shows the experimentally applied lateral force versus top lateral displacements for Repaired Specimen C2. Note that the horizontal force applied to the specimen is not equal to the shear force applied to the specimen, which is presented later (corrections must be applied, in particular to subtract the horizontal components of the vertical actuator forces).

The weld inside the footing in the South web fractured early during the test. This is because the repair weld at the base of the web was not executed as designed and failed prematurely. Therefore, the lateral load capacity of the wall in the negative drift direction was anticipated to be more than what has been obtained experimentally, which was the summation of the two recorded horizontal actuators forces. Hence, in Fig. 16, the applied horizontal force is also compared with twice of the horizontal force from the North actuator (2xNorth) as the weld inside

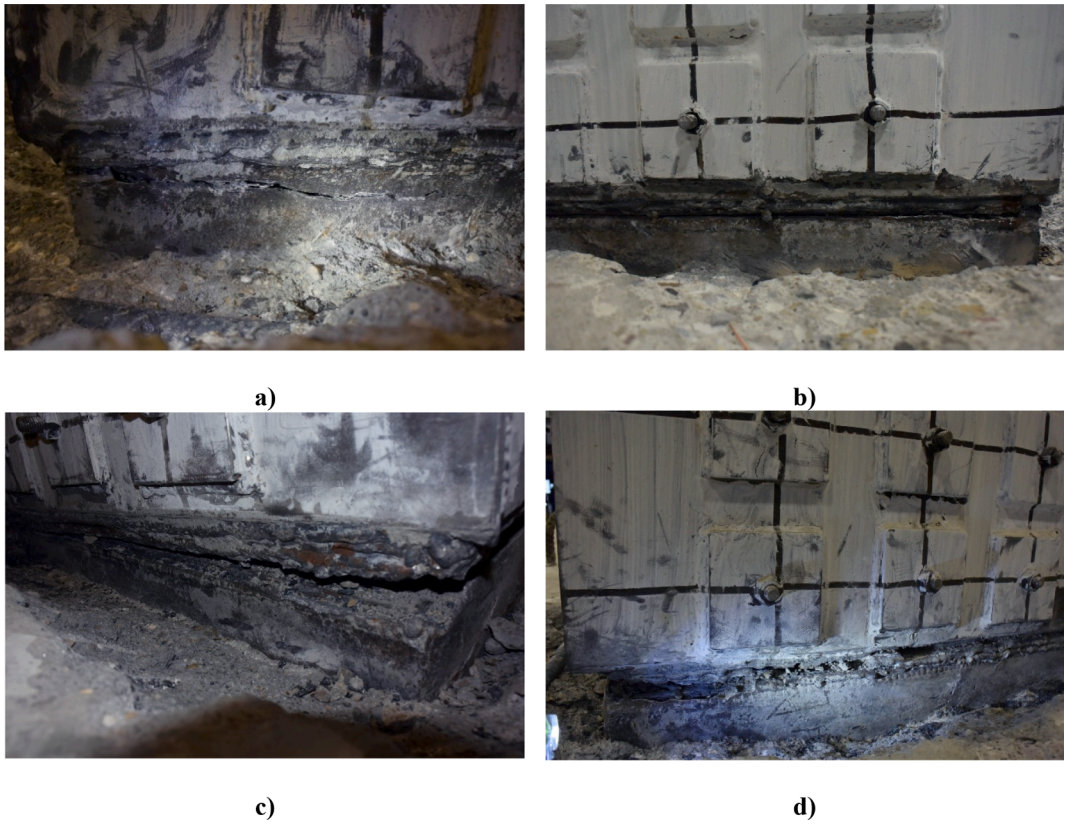

Fig. 14. Weld fractures at a) NWS, b) NWN, c) SWN and d) SWS.

Fig. 15. Close-up picture of the fracture propagation at SWS from a) front view and b) side view.

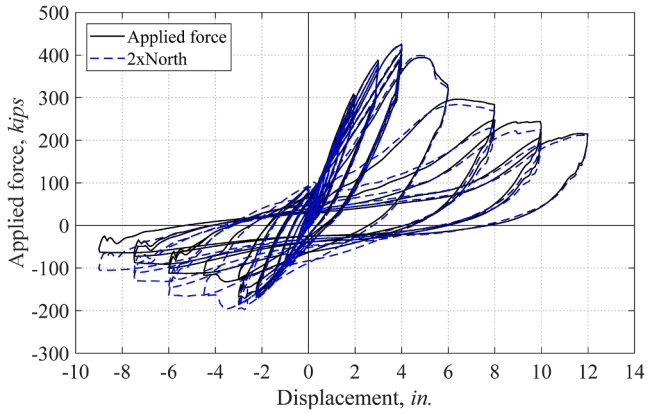

Fig. 16. Experimentally applied lateral force vs. top specimen displacement for Repaired Specimen C2.

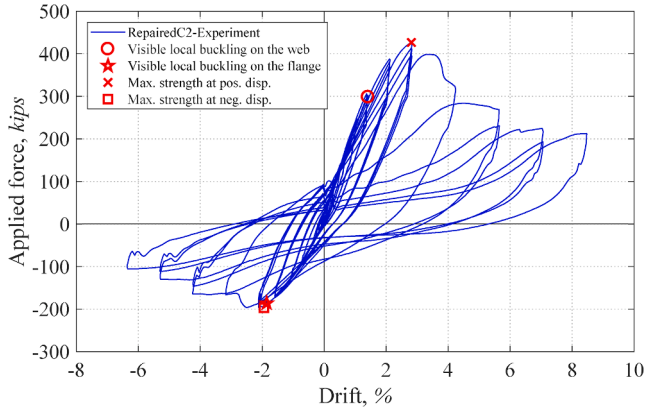

Fig. 17. Some important points marked in the applied lateral force vs. top drift relationship for Repaired Specimen C2.

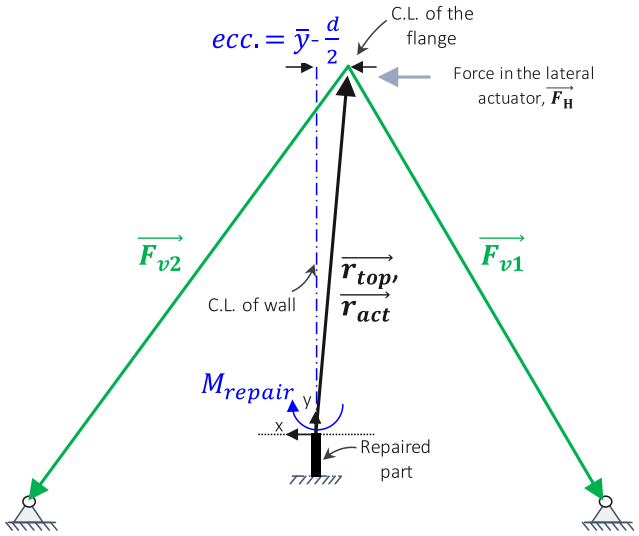

Fig. 18. Equilibrium diagram of the specimen in its initial position.

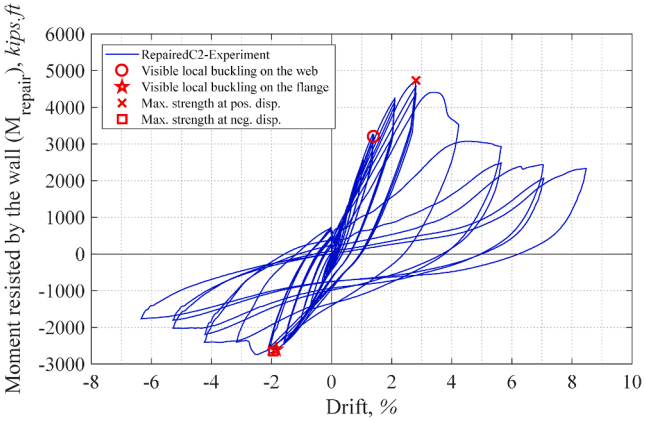

Fig. 19. Moment in wall above repair vs. drift for Repaired Specimen C2.

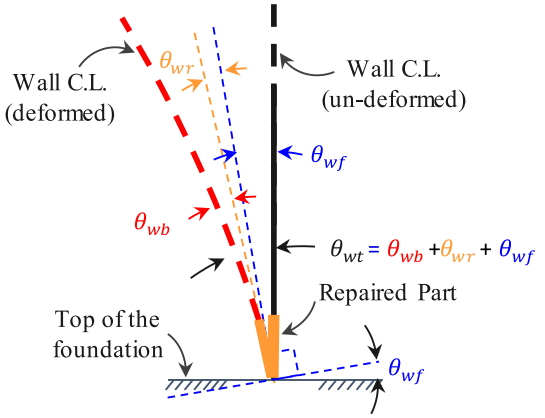

Fig. 20. Components of wall rotation.

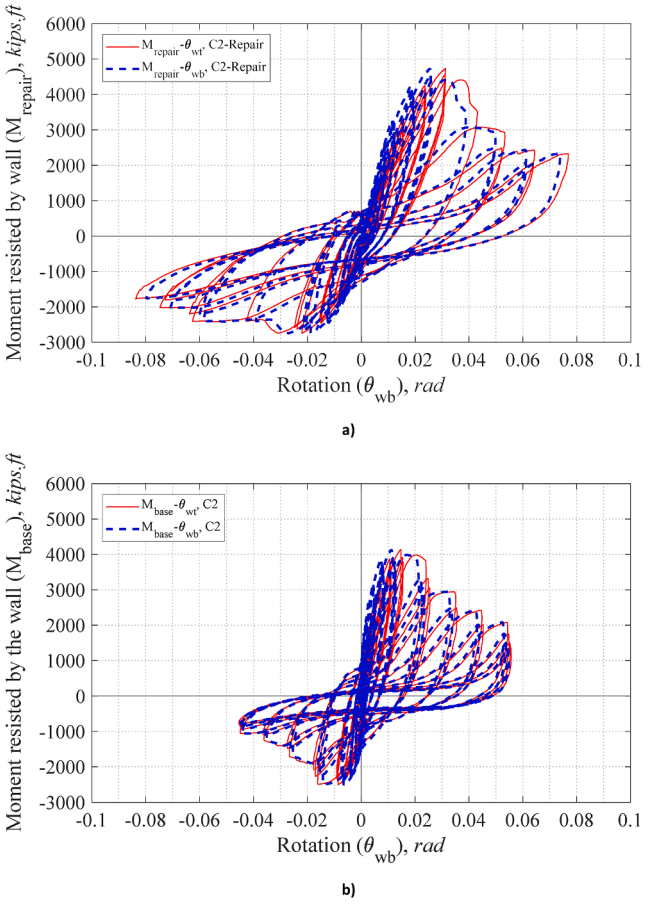

Fig. 21. Base moment vs. total and corrected rotation for a) Repaired Specimen C2 and b) Specimen C2.

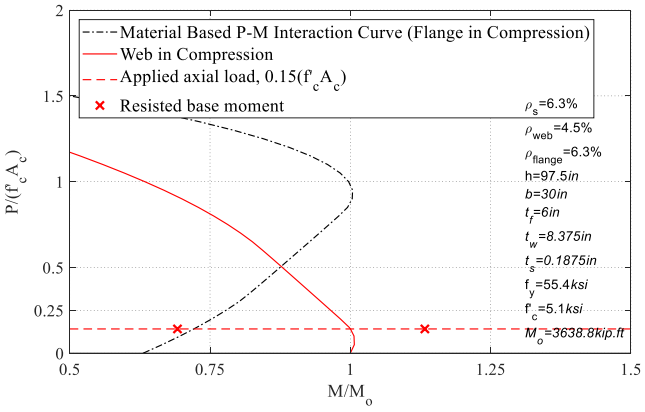

Fig. 22. Comparison of Repaired Specimen C2 flexural strength with P-M interaction curve (where =).

the footing of the North web only fractured at a relatively later stage after much of the expected inelastic action had developed in the plastic hinge location. Given that the applied horizontal forces from both methods are almost the same for the positive drifts, this suggests that the capacity of the wall in the negative direction would have been likewise close to the value obtained as "twice of the horizontal force from the North actuator (2xNorth)" method if early fracture had not happened at the base of the South web, and this was used as a "proxy" for the capacity of the wall in the negative direction.

Building from the results in Fig. 16, Fig. 17 shows the points when the onset of visible local buckling on the web and flange was observed during the test. Note that the lateral drift for the repaired wall is equal to the top of the wall's lateral displacement divided by the distance from the centerline of the lateral actuator to the top of the repaired part (rather than to the base of the wall).

The moment resisted by the wall at the top of the repair was calculated according to the free-body diagram shown in Fig. 18 and by Eq. (1) in order to correct for the eccentricity of the vertical load about the centroid of the wall cross-section, and for the resultant horizontal force from the vertically inclined actuators that the horizontal actuators resisted as the wall drifted during test:

$$\overrightarrow{M_{repair}} = \overrightarrow{r_{act}} \times \overrightarrow{F_H} + \overrightarrow{r_{top}} \times \left(\overrightarrow{F_{v1}} + \overrightarrow{F_{v2}}\right) \quad (1)$$

where $\overrightarrow{M_{repair}}$ is the moment resisted at the top of the repaired part of the wall, $\overrightarrow{r_{act}}$ is the location vector of the horizontal actuator, $\overrightarrow{F_H}$ is the force in the horizontal actuators, $\overrightarrow{r_{top}}$ is the location vector of the top of the wall (at the centroid of flange), and $\overrightarrow{F_{v1}}$ and $\overrightarrow{F_{v2}}$ are the force vectors of the East and West vertically inclined actuator, respectively.

Fig. 19 shows the calculated moment resisted by the wall versus the top of the wall's drift for Repaired Specimen C2.

Ductility of the wall was calculated as the ratio of the ultimate displacement (δ_u) divided by the effective yield displacement ($\delta_{y,eff}$):

$$\mu = \frac{\delta_u}{\delta_{y,eff}} \quad (2)$$

Table 2
Actual, nominal, and expected material properties and calculated flexural resistances for Repaired Specimen C2 (Note: 1 in. = 25.4 mm; 1 ft = 0.3048 m; 1 sq in.=645.2 mm^2; 1 in^4 = 416231 mm^4; 1 psi = 0.0069 MPa; 1 ksi = 6.9 MPa).

Specimen	Material property	Concrete $f_c^{'}$, *ksi*	Steel plates F_y, *ksi*	M_{PSDM}, *kip.ft*		$\frac{M_{experiment}}{M_{PSDM}}$	
				Pos.	Neg.	Pos.	Neg.
Repaired C2	Nominal	6.0	50.0	3567	−2099	1.33	1.32
	Actual	5.1	55.2	3631	−2288	1.30	1.20
	Expected	7.65	55.0	4093	−2322	1.16	1.18

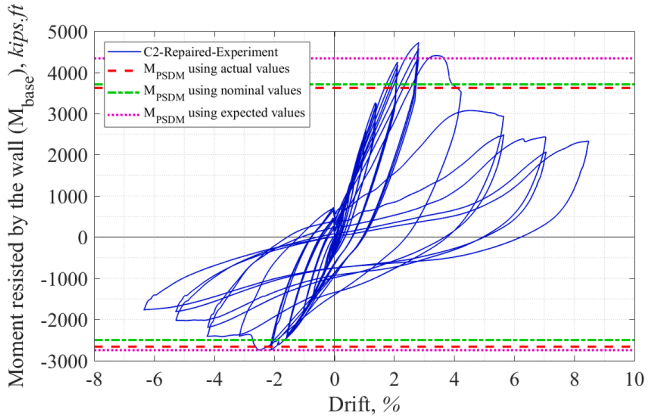

Fig. 23. Comparison of calculated theoretical resistance moments and the experimental base moment for Repaired Specimen C2.

where the ultimate displacement was taken as the value when post-peak flexural strength dropped to 80% of the maximum moment obtained during the test ($M_{repair,\max}$), and the effective yield displacement was taken as the value at the intersection of a horizontal line set at $M_{repair,\max}$ and another one tangent to the initial slope of the resulting pushover curve. Per Eq. (2), a ductility of 2.58/−4.22 was reached in the positive and negative directions for the repaired specimen.

The rotations of the wall above the repair, where plastic hinging developed, was also calculated. Two string pots attached to the wall were used for this purpose: one located *26 in.* (660.4 *mm*) above the top of the repair plate (*49.5 in* (1257.3 *mm*) from the top of the footing), and one *23.5 in* (596.9 *mm*) from the top of the footing. The recorded horizontal displacement of the wall recorded by the first of these two string pots, was divided by its distance to the top of the repair plate (26 *in.* (660.4 *mm*)), which provided the total rotations at the wall base (i.e., θ_{wt}). Note that this calculated rotation also includes both the rotations of the wall-footing connection (i.e., θ_{wf}) and of the repair plate (i.e., θ_{wr}). These two rotations (θ_{wf} and θ_{wr}) were subtracted from the total rotations (θ_{wt}) to obtain the wall rotations at the plastic hinge location (i.e., θ_{wb}). Fig. 20 shows the components of rotations for the repaired wall. A linear rotational spring was used to model the footing and repaired part of wall-to-footing connection at the base of the wall. A line fitted to the M_{base}-θ_{wf} curve corresponding to the linear cycles of the experiment (i.e., until the end of Cycle 7) was used to determine the rotational stiffness of this spring. It was calculated to be 1.113×10^6 *kip.ft/rad* (1.509×10^6 *kN-m/rad*) for Repaired Specimen C2. Unfortunately, the accelerometers placed at South web did not run properly for the first four elastic cycles so the calculated rotation spring stiffness of the foundation in these early cycles was confirmed to remain constant using a LS-DYNA model of the wall. The rotation of the repair part (i.e.,θ_{wr}) was directly obtained by the same procedure used for calculation of the total rotation of the wall above repair, using the horizontal top displacement of the repair plate recorded by the string pot attached to the wall at that location, divided by its distance to the footing's top surface (23.5 *in.*).

Fig. 21a and b shows the calculated moment above repair versus the wall rotations (M_{repair}-θ_{wb}) relationship curve for Repaired Specimen C2 and Specimen C2, respectively. These curves were compared to the one with total rotations above repair (M_{repair}-θ_{wt}) in Fig. 21. Note that since the weld inadequately connecting the splice plate to the existing thicker plate inside footing at South Web of the specimen had fractured before maximum negative moment, the rotations obtained reached 0.08 rad, which is unrealistic based on the results obtained from Specimen C2 (which had maximum rotation of −0.045 *rad* [6]. Therefore, the negative rotations after the point of maximum moment should be ignored. However, at the point when post-peak flexural strength dropped to 80% of the maximum moment obtained during the test, the rotations were 61.7% and 289.7% higher in positive and negative directions, respectively than the original Specimen C2 (0.0356/−0.0596 *rad* in the repaired specimen vs 0.0220/−0.0153 *rad* in Specimen C2). Also, the rotation at which maximum moments was observed was also larger (0.02546/−0.01872 *rad* for the Repaired Specimen C2 and 0.01121/−0.1406 *rad* for Specimen C2). The positive and negative moments were 10–14% more in the repaired specimen (4724/−2746 *kip-ft* (6404.9/–3723.1 *kN-m*) for Repaired Specimen C2 and 4140/−2493 *kip-ft* (5613.1/−3380 *kN-m*) for Specimen C2). This increase in strength could be due to the increase in concrete strength between the time of the original test and test on the repaired specimen, but, unfortunately, no cylinders were left to test the actual strength of the concrete above the repair at the time of testing.

The points of maximum flexural strength experimentally obtained from Repaired Specimen C2 were compared to their corresponding values predicted by theoretical P-M interaction curves as shown in Fig. 22. Strengths obtained from the steel coupons and concrete cylinder tests were used to calculate these P-M interaction curves obtained by fiber section analyses using OpenSees [16]. Results show for the flexure putting the web in compression, the experimentally obtained strength exceeded the value predicted by the interaction diagram based on simple plastic theory. For flexure putting the flange in compression, the experimental value was equal to 87.5% of the value on the interaction diagram.

Table 2 summarizes the nominal, actual, and expected material properties and flexural strengths (taking into accounting axial load applied) calculated using the Plastic Stress Distribution Method (PSDM) for Repaired Specimen C2. Nominal strengths are based on specified material values, namely 50 *ksi* (345 *MPa*) yield for the A572Gr50 steel plates, and 4 *ksi* (27.6 *MPa*) concrete as ordered from the supplier. Expected strengths are obtained when multiplying these values by $R_y = 1.1$ and $R_c = 1.5 \times 0.85$, respectively, in accordance to AISC 341-16 *Seismic Provisions for Structural Steel Buildings*. Actual strengths refer to values calculated on the basis of the wall's web and flanges steel coupons strengths, and of concrete cylinders strengths obtained on the day of the specimen test. The experimentally obtained flexural strengths are also compared to these plastic strength. Comparisons are shown in Fig. 23 for Repaired Specimens C2.

The specimens were inspected after the test. Fig. 24a schematically documents the buckling and fracture damage observed on the steel plates for Repaired Specimen C2. The corresponding pictures of the specimen in all directions are also shown in Fig. 24b. Note that when tie failures were observed, these were due to weld failure at one of their end connections.

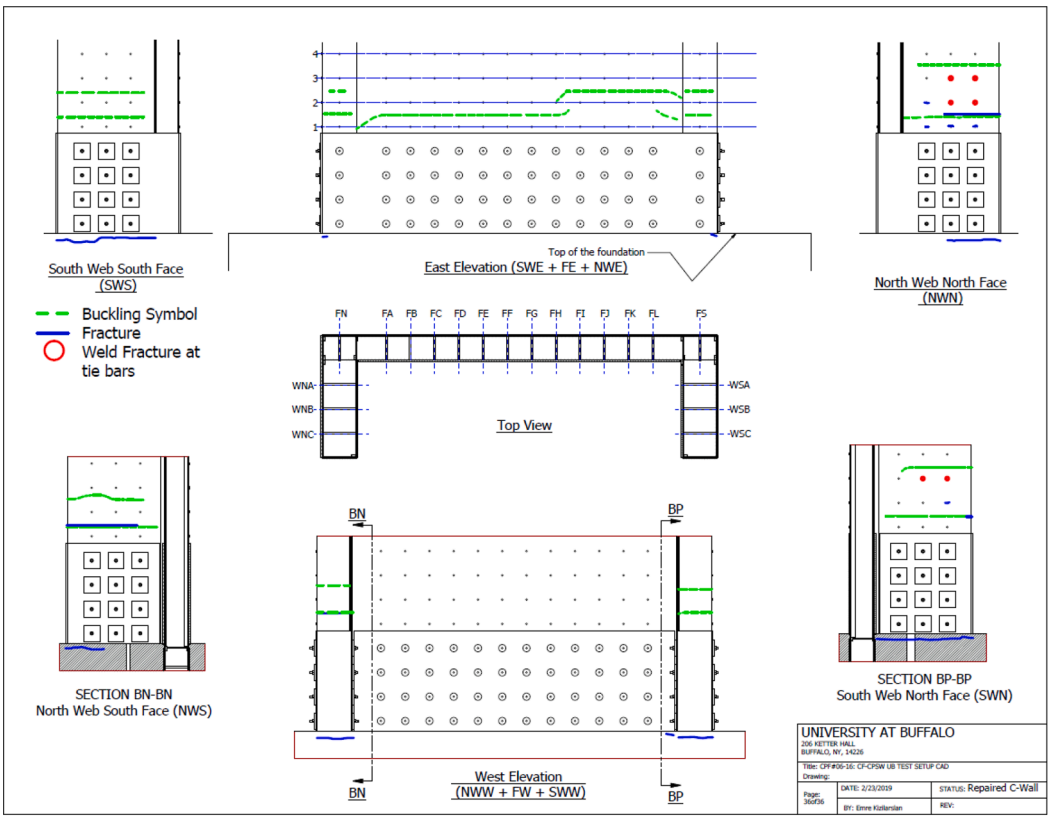

(a)

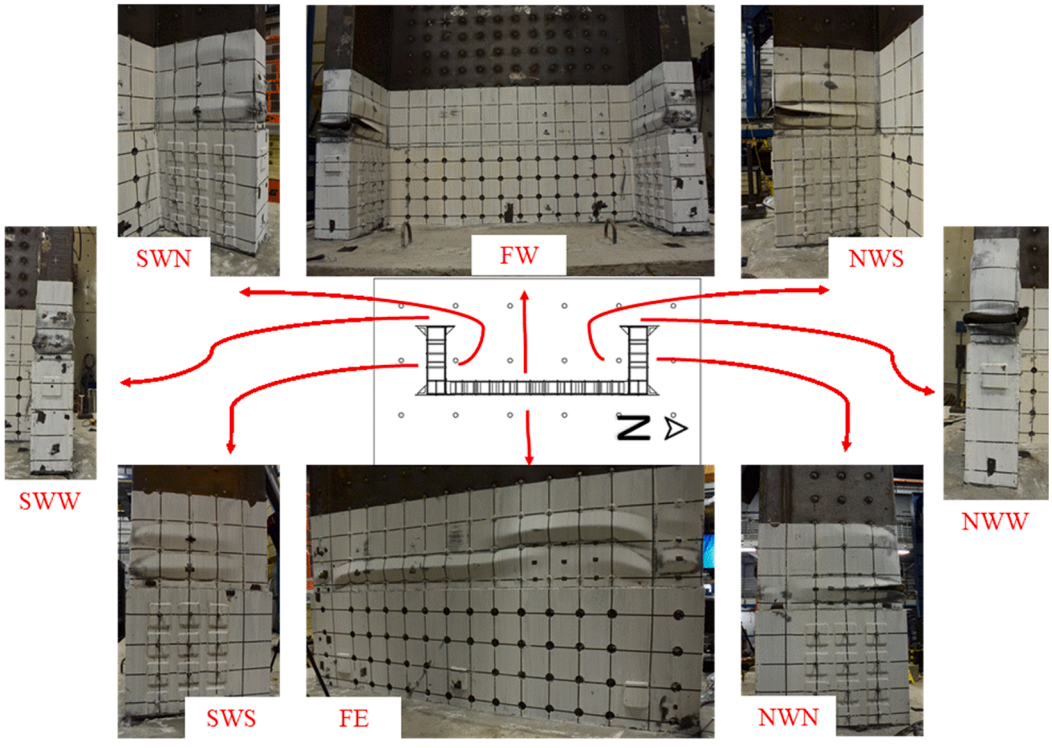

(b)

Fig. 24. Post-test damage inspection of the wall steel plates for Repaired Specimen C2: (a) in sketch, and; (b) in pictures.

9. Summary and conclusions

A large-scale C-shaped Composite Plate Shear Wall/Concrete Filled that had been previously subjected to axial and cyclic flexural loading up to a severe level of damage was repaired and retested, to investigate if this structural system could realistically be returned to a post-earthquake condition having the same capacity for hysteretic behavior. The repaired specimen was subjected to the same loading protocol as the original wall, namely being subjected to 15% of the crushing load of the infill concrete before horizontal cyclic loads were applied.

The repaired specimen exhibited similar yielding, buckling, and fracture behaviors as the originally tested Specimen C2. Ductility reached was 2.58/−4.22 in the positive and negative directions when flexural strength dropped to 80% of the peak value developed, which indicates that the ductility is reduced in the positive direction. This is because the repair weld at the base of one of the webs was not executed as designed and failed prematurely. Nonetheless, the repaired specimen (like the unrepaired one did) reached or exceeded its calculated plastic moment capacities in the positive and negative direction. However, due to the fracture at the weld inside of the footing between the existing steel plate of Specimen C2 and its repair plate, the data obtained in the negative direction for the Repaired Specimen C2 is not deemed to be representative beyond a drift of 1.8% (Cycle18) and a moment equal to 115% of M_p as the rotations obtained reached 0.08 rad, which is unrealistic based on the results obtained from Specimen C2 (which had maximum rotation of −0.045 rad [6]. More specifically:

- Maximum strength was reached at a positive drift of 2.1% for both Specimen C2 and Repaired Specimen C2.
- Tests showed that, as was the case for Specimen C2, local buckling in Repaired Specimen C2 started in the cycles after yielding, with minor reduction in wall strength due to buckling alone.
- The fracture of the steel plate was progressive and dominantly responsible for the loss in flexural strength.
- Buckling was observed to occur between multiple layers of tie bars. This is because yielding spread over a substantial part of the wall height.

Overall, results indicate that C-shaped Composite Plate Shear Walls/Concrete-filled (C-SPW/CF) repaired by the procedure adopted here can exhibit a good cyclic inelastic behavior without premature flexural strength degradation, while resisting an axial load equal to 15% $A_c f'_c$.

CRediT authorship contribution statement

Emre Kizilarslan: Validation, Investigation, Formal analysis, Data curation, Writing - original draft, Writing - review & editing, Visualization, Conceptualization. **Michel Bruneau:** Supervision, Project administration, Writing - review & editing, Visualization, Conceptualization, Methodology, Funding acquisition.

Declaration of Competing Interest

The authors declare that they have no known competing financial interests or personal relationships that could have appeared to influence the work reported in this paper.

Acknowledgments

This research was supported by the Charles Pankow Footing (CPF) and the American Institute of Steel Construction (AISC), through CPF research grant #06-16 awarded to co-PIs Amit Varma, from Purdue University, and Michel Bruneau, University at Buffalo. The work reported here focuses on the part of the research project conducted at the University at Buffalo only. The researchers also thank Magnusson Klemencic Associates (MKA), Cives Steel Co., J.F.Stearns Co., and Turner Construction, for the donated steel and fabrication of the test specimens. The researchers are also thank the Project Advisory Team members (Ron Klemencic, *Chairman & CEO,* Magnusson Klemencic Associates (MKA); Jim Malley, *Senior Principal,* Degenkolb Engineers; Ron Hamburger, *Senior Principal*, Simpson Gumpertz & Hager; Larry Kruth, *Vice President,* American Institute of Steel Construction (AISC); Devin Huber, *Director of Research*, AISC, and; Peter Timler, *President*, West-Cascadia Consultants) for their technical guidance.

References

[1] MSC. 850-FT-TALL RAINIER SQUARE TOWER TOPS OUT IN ONLY 10 MONTHS. Modern Steel Construction; 2019. Retrieved from: https://www.aisc.org/modernsteel/news/2019/august/rainier-square-tower-tops-out-at-850-ft-in-under-10-months/.
[2] Bowerman H, Chapman JC. Bi-steel steel-concrete-steel sandwich construction. Compos Constr Steel Concret IV 2002:656–67.
[3] Bhardwaj SR, Varma AH. Design of modular steel-plate composite walls for safety-related nuclear facilities. American Institute of Steel Construction; 2017.
[4] Varma AH, Malushte SR, Sener K, Lai Z. Steel-plate composite (SC) walls for safety related nuclear facilities: design for in-plane and out-of-plane demands. In: Proceedings of the 21st IASMiRT Conference (SMiRT 21).
[5] Varma AH, Malushte SR, Sener KC, Lai Z. Steel-plate composite (SC) walls for safety related nuclear facilities: design for in-plane forces and out-of-plane moments. Nucl Eng Des 2014;269:240–9.
[6] Kenarangi H, Kizilarslan E, Bruneau M. Cyclic behavior of c-shaped composite plate shear walls–concrete filled. Eng Struct 2020;226:111306.
[7] Shafaei S, Varma AH, Seo J, Klemencic R. Cyclic Lateral Loading Behavior of Composite Plate Shear Walls/Concrete Filled (C-PSW/CF). J Struct Eng, ASCE, submitted for review, 2020.
[8] Alzeni Y, Bruneau M. Cyclic Inelastic Behavior Of Concrete Filled Sandwich Panel Walls Subjected To In-Plane Flexure. Technical Rep. MCEER 14-009, MCEER The State University of New York at Buffalo; 2014.
[9] Kenarangi H, Bruneau M. Experimental study on composite action in reinforced concrete-filled steel-tube shaft foundations. J Bridge Eng 2019;24(7):04019060.
[10] Lehman DE, Roeder CW. Foundation connections for circular concrete-filled tubes. J Constr Steel Res 2012;78:212–25.
[11] Bruneau M, Kizilarslan E. Seismic and Wind Behavior and Design of Coupled CF-CPSW Core Walls for Steel Buildings. Interim Report No.5 to Charles Pankow Foundation: Grant # 06-15; 2019.
[12] El-Bahey S, Bruneau M. Bridge piers with structural fuses and bi-steel columns. I: Experimental testing. J Bridge Eng 2011;17(1):25–35.
[13] Fujimoto M, Wada A, Saeki E, A., W., Y., H. A study on the unbonded brace encasted in bucking-restrained concrete and steel tube. J Str Eng, AIJ, 34; 1988.
[14] Iwata M, Kato T, Wada A. Buckling-restrained braces as hysteretic dampers. Behavior of Steel Structures in Seismic Areas 2000:33–8.
[15] Saeki E, Maeda Y, Nakamura H, Midorikawa M, Wada A. Experimental study on practical-scale unbonded braces. J Struct Constr Eng, Architectural Institute of Japan 1995;476:149–58.
[16] McKenna F, Mazzoni S, Fenves G. Open System for Earthquake Engineering Simulation (OpenSees) Software Version 2.2. 5. University of California, Berkeley, CA; 2016. Available from http://opensees.berkeley.edu.